Polynuclear and Extended Coordination Compounds from Preorganized Bimetallic Components: Tuning the Magnetic Properties of Dinickel(II) Building Blocks

Guido Leibeling,[a] Serhiy Demeshko,[a] Bernhard Bauer-Siebenlist,[a] Franc Meyer,*[a] and Hans Pritzkow[b]

Keywords: Molecular magnetism / Nickel / Dinuclear complexes / Tetranuclear complexes / Magnetic properties / Azides

Various dinucleating pyrazole ligands with chelating side arms in the 3- and 5-positions of the heterocycle have been shown to form Ni^{II}/azido complexes, where the metal ions are spanned by the pyrazolate, and an azido bridge. Four new complexes have been characterized by X-ray crystallography and variable-temperature magnetic susceptibility studies. The Ni···Ni distance, and hence the intra-dimer coordination mode of the azide (μ-1,1 or μ-1,3), is determined by the chelate arm length, such that the magnetic properties of the bimetallic units can be controlled. The intramolecular coupling between the Ni^{II} (S = 1) ions was found to be ferromagnetic (J = +4.0 ± 0.5 cm^{-1}) in the case of $[L^1Ni_2(N_3)(NO_3)_2]$ (**1**) with a μ-1,1 azide, but antiferromagnetic (J = −25.7 ± 0.3 cm^{-1}) for $[L^2Ni_2(N_3)](ClO_4)_2$ (**2**) with a μ-1,3 azide. Such bimetallic units can serve as building blocks for the construction of high-nuclearity Ni^{II}/azide compounds, as demonstrated for the tetranuclear complexes $[L^1_2Ni_4(\mu\text{-}1,1\text{-}N_3)_2(\mu\text{-}1,3\text{-}N_3)_2](BPh_4)_2$ (**3**), and $[L^3Ni_2(N_3)_3]_2$ (**4**). Complex **3** was obtained by the replacement of the labile nitrates in **1** by additional azido ligands, that bridge the two $[L^1Ni_2(N_3)]^{2+}$ subunits in the μ-1,3 mode. Complex **4** incorporates two additional azides, and two of its azido linkages were found in the rare μ-1,1,3 binding mode (albeit with relatively long Ni–N bond lengths). The magnetic properties of the tetranuclear species were as predicted from the building blocks and the respective azide binding, with ferromagnetic intra-dimer and antiferromagnetic inter-dimer exchanges, yielded an overall S = 0 ground state.
(© Wiley-VCH Verlag GmbH & Co. KGaA, 69451 Weinheim, Germany, 2004)

Introduction

Recent years have seen extensive studies of the magnetic properties of polynuclear metal complexes with exchange coupled magnetic centers.[1,2] With the objective of obtaining nanoscale molecular magnets, current activities focus on increasing the nuclearity of single-molecule clusters, that have ground electronic states with a large spin[3] and enhancing the anisotropy of single-molecule type systems.[4] In relation to the latter, nickel(II) is a preferred spin carrier due to its large single-ion zero-field splitting. Also, the flexidentate azido ligand is frequently being used as a bridging ligand, since it provides coordination compounds with great structural variety and efficiently mediates different kinds of magnetic exchange depending on its mode of coordination.[5] The favorable combination of nickel(II) ions and azide ligands has indeed provided a variety of molecular architectures in which the azide normally adopts one of its common bridging modes.[6] These are the μ-1,1 mode (*end-on*, Figure 1), which usually results in ferromagnetic coupling, and the μ-1,3 mode (*end-to-end*), which in most cases gives rise to antiferromagnetic behavior. Other triply or quadruply bridging azide coordination modes such as μ_3-1,1,1, μ_3-1,1,3, μ_4-1,1,1,1 or μ_4-1,1,3,3 have remained relatively scarce,[7−9] although these are of particular interest with respect to the construction of high-nuclearity complexes or polymeric systems.

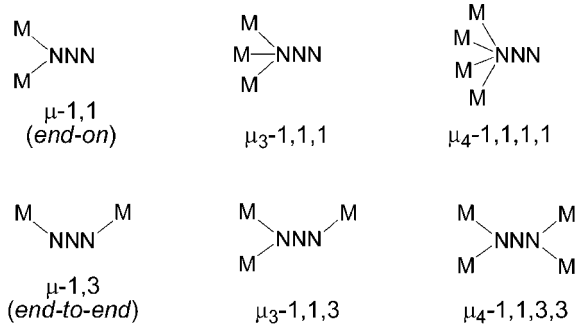

Figure 1. Azide bridging modes

A major task in the rational design of nickel/azide-based coordination compounds with predictable magnetic properties is the control of the azide bridging mode and, even

[a] Institut für Anorganische Chemie, Georg-August-Universität, Tammannstrasse 4, 37077 Göttingen, Germany
Fax: (internat.) + 49-(0)551-393063
E-mail: franc.meyer@chemie.uni.goettingen.de
[b] Anorganisch-Chemisches Institut der Universität Heidelberg, Im Neuenheimer Feld 270, 69120 Heidelberg, Germany

more demanding, the direct assembly of larger complexes with a desired nuclearity and topology. It is not so long ago, however, that a review article started it would be impossible to synthetically determine which coordination mode of the azide linkage would be adopted.[6] The aim of the present work here is twofold. Firstly, it is demonstrated that the azide binding mode in the bimetallic pocket of a preorganized dinickel(II) array, and hence the magnetic properties of the dinuclear compound, can be selectively altered by appropriate changes to the dinucleating ligand scaffold. Secondly, it is shown that such bimetallic units can serve as building blocks for the targeted construction of tetranuclear species with significant magnetic coupling.

Results and Discussion

Synthesis and Characterization of Complexes

A set of compartmental pyrazolate-based ligands HL^1, HL^2, and HL^3 was chosen as dinucleating scaffolds for this work (Figure 2). These three ligands differ in the number of N-donor sites in their chelate side arms (HL^1 versus HL^3), as well as by the side arm chain length (HL^1 versus HL^2). The latter was previously shown to determine the metal-metal separation in the resultant bimetallic complexes. Whereas the longer ligand side arms in HL^1 allow the metal ions to approach relatively close to distances of about 3.5 Å, the shorter side arms in HL^2 pull the metal ions back and apart, thereby enforcing metal-metal distances above 4 Å.[10] This has drastic consequences for an azide co-ligand accommodated within the bimetallic pocket, since the larger metal-metal separation will necessarily lead to an *end-to-end* coordination, whereas the shorter metal-metal separation should only be suitable for an *end-on* bound azide. Dinickel(II) complexes of the related ligand HL^4 have previously proved valuable as building blocks for the controlled synthesis of structurally alternating 1D chains (*J*-alternating chains),[11,12] with the expected μ-1,3 azide coordination within the bimetallic entities.[12]

These considerations were confirmed by the X-ray crystallographic findings for complexes $[L^1Ni_2(N_3)(NO_3)_2]$ (**1**) and $[L^2Ni_2(N_3)](ClO_4)_2$ (**2**), both of which were obtained in a straightforward manner from the respective ligand, one equivalent of base, one equivalent of NaN_3, and two equivalents of a nickel salt such as $Ni(NO_3)_2{\cdot}6H_2O$ or $Ni(ClO_4)_2{\cdot}6H_2O$. The molecular structures of **1** and of the cation of **2** are depicted in Figure 3 and 4, respectively, along with selected bond distances and angles.

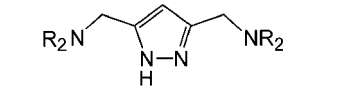

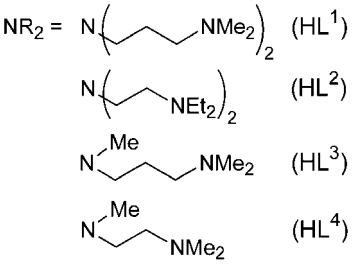

Figure 2. Ligands used in this work

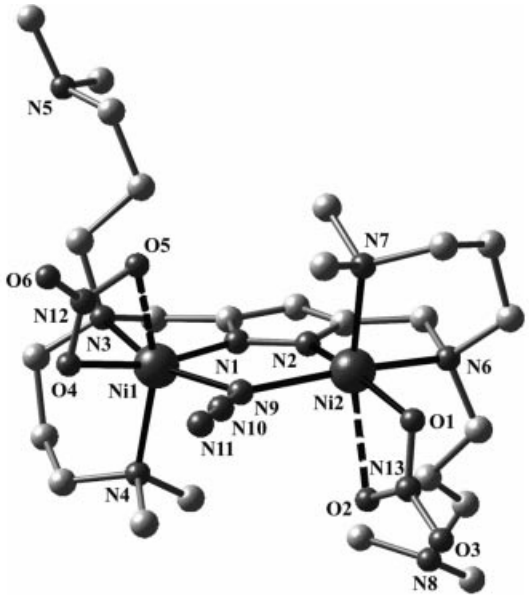

Figure 3. View of the molecular structure of **1**. In the interests of clarity all hydrogen atoms have been omitted. Selected bond distances (Å) and angles (°): Ni1−N1 1.928(1), Ni1−O4 2.070(1), Ni1−N4 2.102(1), Ni1−N9 2.162(1), Ni1−N3 2.222(1), Ni1−O5 2.298(1), Ni2−N2 1.943(1), Ni2−O1 2.061(1), Ni2−N7 2.094(1), Ni2−N9 2.151(2), Ni2−N6 2.235(1), Ni2−O2 2.350(2), Ni1···Ni2 3.660(2), N9−N10 1.212(2), N10−N11 1.150(2); Ni1−N9−Ni2 116.12(6), Ni1−N9−N10 118.22(12), Ni2−N9−N10 124.83(12)

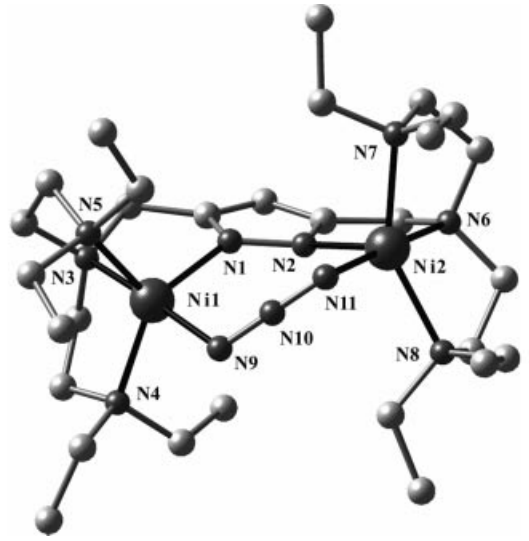

Figure 4. View of the molecular structure of the cation of **2**. In the interests of clarity all hydrogen atoms have been omitted. Selected bond distances (Å) and angles (°): Ni1−N1 2.013(2), Ni1−N9 2.065(2), Ni1−N3 2.087(2), Ni1−N4 2.105(4), Ni1−N5 2.123(2), Ni2−N2 2.007(2), Ni2−N11 2.059(2), Ni2−N6 2.095(2), Ni2−N7 2.121(2), Ni2−N8 2.155(2), Ni1···Ni2 4.421(2), N9−N10 1.178(2), N10−N11 1.179(2); Ni1−N9−N10 114.81(13), Ni2−N11−N10 113.75(13)

 © 2004 Wiley-VCH Verlag GmbH & Co. KGaA, Weinheim

In complex **2**, both nickel ions are nested within their respective coordination compartments, and are five-coordinate (intermediate between TBP-5 and SP-5: τ = 0.60/0.52)[13] with the azide bound in the anticipated *end-to-end* fashion within the bimetallic pocket. While certainly too large to allow for μ-1,1 azide binding, the Ni···Ni distance of 4.421 Å in **2** is still relatively short for a μ-1,3 azide linkage and thus causes the linear azide to tilt severely with respect to the pyrazolate plane. At the same time, the metal ions are forced out of that plane in order to allow for reasonable Ni1−N9−N10 and Ni2−N11−N10 bond angles of 114.8(5)° and 113.8(5)°, respectively. In the absence of geometric constraints by a dinucleating ligand framework, much wider Ni−N−N_{azide} angles are usually observed (>120°). These particular geometric constraints of the [L^2Ni_2] scaffold have previously led to the identification of an extremely bent cyanide coordination within its bimetallic pocket.[14]

In contrast to **2**, the longer ligand side arms in **1** give rise to a much shorter Ni···Ni distance of 3.660 Å. This induces incorporation of the azide in a μ-1,1 mode and a rather relaxed binding situation, as judged from the fact that both nickel ions as well as the azide-N9 centers are located roughly within the plane of the pyrazolate heterocycle. The almost linear azide makes an angle of ≈ 7° with that plane. While the N_3 unit is symmetric in **2** [*d*(N−N) = 1.178(2)/1.179(2) Å], it is distinctly asymmetric in **1** [*d*(N9−N10) = 1.212(2) Å, *d*(N10−N11) = 1.150(2) Å]. Interestingly, the lower stability of the six-membered chelate rings in **1** allows the nitrate anions to displace one side arm donor at each nickel, which is left uncoordinated and dangling. The nitrates are found semi-chelating with one short [2.061(1)/2.070(1) Å], and one much longer [2.350(2)/2.298(1) Å] N−O bond. Unfortunately, we have not been able to grow single crystals of a $[L^1Ni_2(N_3)]^{2+}$ complex with weakly coordinating counterions such as ClO_4^- or BPh_4^-.

Despite the different binding modes of the azide ligands in **1** and **2**, their $\nu_{as}(N_3)$ stretches are similar (Table 1). Binding of the azide and the nitrates in **1** is apparently of comparable strength, since both $[L^1Ni_2(N_3)(NO_3)]^+$ and $[L^1Ni_2(NO_3)_2]^+$ are found as dominant ions in the FAB mass spectrum of the complex. It was thus tempting to provide additional potentially bridging azide ions instead of the nitrates, in order to assemble two (or even more) dinuclear units $[L^1Ni_2(\mu\text{-}1,1\text{-}N_3)]^{2+}$ into larger nickel/azido complexes. A similar strategy has recently been reported to provide tetranuclear nickel(II) complexes from coordinatively unsaturated thiophenolate-based dinickel(II) building blocks or some pyrazolate-based tetranickel(II) complexes with novel azide binding.[9,15] This procedure also proved successful in the present case, since treatment of $[L^1]^-$ with two equivalents of Ni^{2+} and two equivalents NaN_3 gave the tetranuclear species **3**, which could be crystallized as its BPh_4^--salt. The molecular structure of the cation is displayed in Figure 5, along with selected metric parameters.

Table 1. Selected IR absorptions of complexes **1**−**4**, in cm^{-1}

Complex	$\nu_{as}(N_3)$
1	2058 (s)
2	2067 (s)
3	2129 (s), 2064 (m)
4	2103 (s), 2055 (s), 2037 (s)

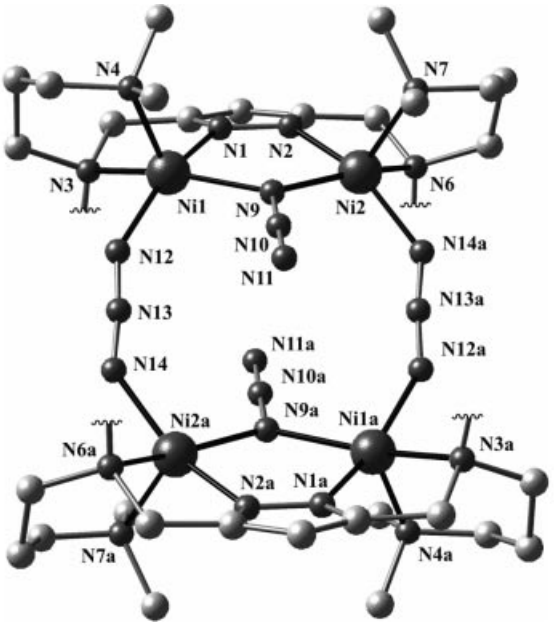

Figure 5. View of the molecular structure of the cation of **3**. In the interests of clarity all hydrogen atoms and the dangling ligand side arms attached to N3 and N6 have been omitted. Selected atom distances (Å) and angles (°): Ni1−N1 1.946(1), Ni1−N12 2.037(2), Ni1−N4 2.064(2), Ni1−N9 2.119(2), Ni1−N3 2.165(2), Ni2−N2 1.945(2), Ni2−N14 2.026(2), Ni2−N7 2.074(2), Ni2−N9 2.120(2), Ni2−N6 2.174(2), Ni1···Ni2 3.639(2), Ni1···Ni2a 5.788(2), Ni1···Ni1a 6.719(2), N9−N10 1.196(2), N10−N11 1.143(2), N12−N13 1.158(2), N13−N14 1.166(2); Ni1−N9−Ni2 118.31(7), N12−N13−N14 174.5(2)

In **3**, two dinuclear $[L^1Ni_2(\mu\text{-}1,1\text{-}N_3)]^{2+}$ entities are linked through two μ-1,3 azide ions to give a rectangular tetranuclear species with crystallographic C_i symmetry. Complex **3** is formally derived from the aggregation of two complexes **1** via replacement of the semi-chelating nitrates by the μ-1,3 bridging azides. Indeed, each pyrazolate-based bimetallic subunit of **3** is basically similar to the dinuclear complex **1** and exhibits a similar Ni···Ni distance [3.639(2) Å], although in this case the nickel and μ-1,1 azide ions are somewhat more displaced out of the plane of the pyrazolate heterocycle and the two dangling side arms are found on the same side of the dinuclear component. The separation of the nickel ions spanned by the μ-1,3-N_3 is 5.788(2) Å. While the μ-1,1 azide is again highly asymmetric [*d*(N9−N10) = 1.196(2) Å versus *d*(N10−N11) = 1.143(2) Å], the μ-1,3 azide is almost symmetric [*d*(N12−N13) = 1.158(2) Å versus *d*(N13−N14) = 1.166(2) Å].

Since one side arm of each ligand coordination compartment remains uncoordinated in **3**, it seemed appropriate to also attempt to employ the related bis(tridentate) ligand

 © 2004 Wiley-VCH Verlag GmbH & Co. KGaA, Weinheim

$[L^3]^-$ for the preparation of similar polynuclear complexes. To this end, a tetranickel(II) complex was obtained from the reaction of $[L^3]^-$ with $Ni(ClO_4)_2 \cdot 6H_2O$ and NaN_3. However, in this case the product $[L^3Ni_2(N_3)_3]_2$ (**4**) is neutral due to the coordination of additional azide ions. The structure of **4** was elucidated by X-ray crystallography, and is depicted in Figure 6 together with selected bond distances and bond angles.

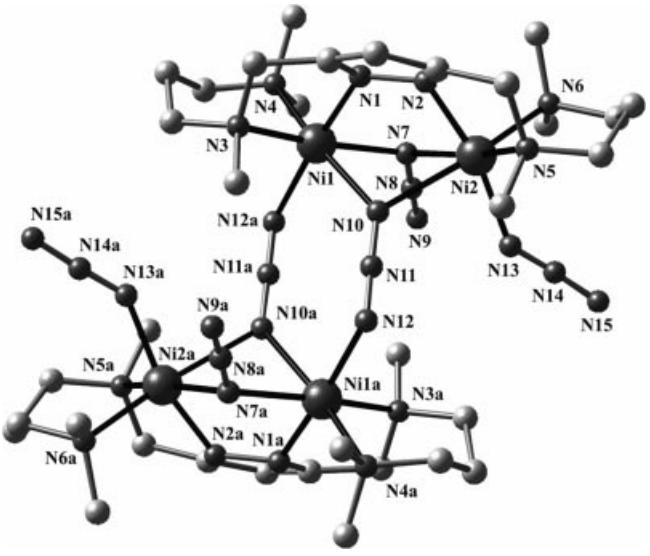

Figure 6. View of the molecular structure of **4**. In the interests of clarity all hydrogen atoms have been omitted. Selected atom distances (Å) and angles (°): Ni1−N1 1.995(3), Ni1−N12a 2.066(3), Ni1−N4 2.141(3), Ni1−N7 2.147(3), Ni1−N3 2.179(3), Ni1−N10 2.310(3), Ni2−N2 2.004(3), Ni2−N13 2.028(3), Ni2−N6 2.128(3), Ni2−N7 2.148(3), Ni2−N5 2.178(3), Ni2−N10 2.443(3), Ni1···Ni2 3.350(3), Ni1···Ni1a 5.358(3), Ni1···Ni2a 5.913(3), N7−N8 1.207(4), N8−N9 1.153(4), N10−N11 1.176(4), N11−N12 1.168(4), N13−N14 1.134(4), N14−N15 1.163(5); Ni1−N7−Ni2 102.49(12), Ni1−N10−Ni2 89.57(10)

Again, complex **4** is composed of two pyrazolate-based dinuclear components $[L^3Ni_2(\mu\text{-}1,1\text{-}N_3)]^{2+}$, that are linked by two further azides. Due to the presence of a fifth and sixth azide, which bind terminally to Ni2, however, the N_3^- group linking the bimetallic subunits is shifted from the μ-1,3 position in **3** to a μ_3-1,1,3 position in **4**. All metal centers are thus six-coordinate in **4** but five-coordinate in **3**. Triply bridging μ_3-1,1,3 azide ions are scarce, and in most cases exhibit two rather long $N_{azide}-M$ bonds,[9,16] as can also be observed in **4** [*d*(Ni1−N10) = 2.310(3) Å and *d*(Ni2−N10) = 2.433(3) Å, in contrast to *d*(Ni1−N12a) = 2.066(3) Å]. Complex **4** enables a comparison to be made of the metric parameters for three different types of N_3^- ligands in a single compound. N−N bond lengths are clearly elongated for the μ-1,1 and μ_3-1,1,3 bridges compared with the terminal N_3^-, and the asymmetry is least pronounced in the μ_3-1,1,3 azide [1.168(4)/1.178(4) Å versus 1.153(4)/1.207(4) Å in the μ-1,1 azide and 1.134(4)/1.163(5) Å for the terminal azide]. It seems reasonable to assign the high-energy IR bands for $\nu_{as}(N_3)$ at 2129 (**3**) and 2103 cm^{-1} (**4**) to the μ-1,1 and μ-1,1,3 azido ligands, respectively (Table 1).

Magnetic Properties

For all complexes, the magnetic susceptibility measurements were carried out at two different magnetic fields in a temperature range from 2.0 K to 295 K (300 K). No significant field dependence was observed for any of the complexes.

The temperature dependence of the magnetic susceptibility χ_M, and of the product $\chi_M T$ for the dinuclear complexes **1** and **2** are shown in Figure 7 and 8, respectively. As would be expected from the different binding modes of the azide bridge, the magnetic properties of the two compounds differ fundamentally. In the case of **1**, the observed $\chi_M T$ value of 2.66 $cm^3 \cdot K \cdot mol^{-1}$ (4.62 μ_B) at room temperature remains nearly constant down to 100 K. Below this temperature $\chi_M T$ gradually increases, reaching a maximum of 3.13 $cm^3 \cdot K \cdot mol^{-1}$ (corresponding to a μ_{eff} value of 5.01 μ_B) at 12 K, indicating ferromagnetic exchange. At even lower temperatures, $\chi_M T$ drops rapidly, which may be due to the effects of zero-field splitting or intermolecular antiferromagnetic interactions.

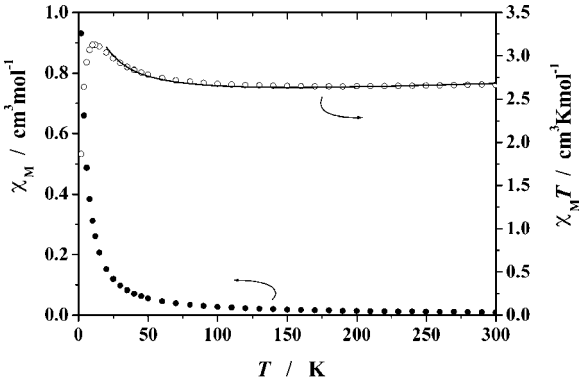

Figure 7. Plot of χ_M (solid circles) and $\chi_M T$ (open circles) vs. *T* for **1** at 2000 G. The solid line represents the calculated curve fit (see text)

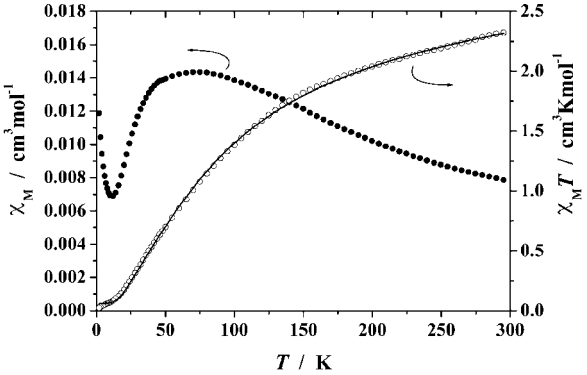

Figure 8. Plot of χ_M (solid circles) and $\chi_M T$ (open circles) vs. *T* for **2** at 2000 G. The solid line represents the calculated curve fit (see text)

The experimental data for **1** were modeled in the range from 300 K to 20 K using Equation (1)[1b] deduced from the Hamiltonian $H = -2JS_1S_2$, with additional terms accounting for small amounts of paramagnetic impurities (ρ), and

 © 2004 Wiley-VCH Verlag GmbH & Co. KGaA, Weinheim

for the temperature independent paramagnetism (*TIP*). A satisfactory fit was obtained with the parameters $g = 2.25 \pm 0.01$ and $J = +4.0 \pm 0.5$ cm^{-1} ($\rho = 2\%$, $TIP = 6.0 \times 10^{-4}$ cm^3·mol^{-1}), confirming moderate ferromagnetic coupling. Owing to the likely occurrence of zero-field splitting at low temperatures, however, the magnitude of J should be interpreted with caution.

$$\chi_M = \frac{Ng^2\mu_B{}^2}{kT}\frac{2e^{2(J/kT)} + 10e^{6(J/kT)}}{1 + 3e^{2(J/kT)} + 5e^{6(J/kT)}}(1-\rho) + \frac{2Ng^2\mu_B{}^2}{3kT}\rho + TIP \quad (1)$$

For complex **2** the observed $\chi_M T$ value at 295 K is 2.32 cm^3·K·mol^{-1} (4.31 μ_B). It drops steadily with decreasing temperature, and finally tends to zero, indicating an $S = 0$ ground state. This behavior is typical for dinuclear complexes with intramolecular antiferromagnetic coupling. The experimental magnetic data for **2** were modeled in the range from 295 K to 2 K using Equation (1),[1b] which gives the fit parameters $g = 2.28 \pm 0.02$, $J = -25.7 \pm 0.3$ cm^{-1}, $\rho = 5.7 \pm 0.1\%$, and $TIP = 7.9 \times 10^{-4}$ cm^3·mol^{-1}.

A number of dinuclear nickel(II) complexes with only a single μ-1,3 azido bridge have been characterized magnetically.[17] Two geometric parameters, the angles Ni−N−N and the dihedral angle φ along the azide ligand, are often considered for magnetostructural correlations.[6] For a Ni−N_3−Ni torsion angle of φ = 180°, the antiferromagnetic coupling can be predicted to have a maximum at Ni−N−N angles around 108°, and to decrease at larger angles. On the other hand, for all Ni−N−N angles, the maximum coupling would be expected for a torsion angle of 180°. However, the effect of torsion should be less pronounced than the effect of the bond angle. In the absence of any constraining ligand scaffold, Ni−N−N angles tend to lie in the range 130°−145° with φ = 180°, resulting in J values in the range of −8 to −22 cm^{-1}.[6,18] In view of the very acute Ni−N−N angles (114.8° and 113.7°), and the fact that φ = 55.4° for **2**, a J value even more negative than the lower limit of the above range was thus expected, in good agreement with experimental findings. Although some contribution from the pyrazolate is certainly present, the azide appears to provide the dominant pathway for the antiferromagnetic exchange coupling.

Dinuclear nickel(II) complexes with two *end-on* azido bridges and a {Ni(μ−1,1−N_3)$_2$Ni} central core generally feature Ni−N−Ni angles θ in the narrow range 101−105°, and J values between +13 and +37 cm^{-1}.[6,18] DFT calculations have suggested a clear correlation between the exchange coupling and θ, with the interaction predicted to be ferromagnetic for all the range of θ angles explored.[19] For the {Ni(μ-1,1-N_3)$_2$Ni} core, a maximum is expected when θ ≈ 104°. On the other hand, the out-of-plane displacement of the azide should only have a minor influence. The Ni1−N9−Ni2 angle induced by the dinucleating ligand scaffold in **1** is unusually large [116.12(6)°], and a small J value could thus be expected for the single μ-1,1 azide, in accordance with experimental results. Despite this, and despite a likely antiferromagnetic contribution from the pyrazolate bridge, however, the exchange in **1** is still clearly ferromagnetic.

Complex **3** features a $\chi_M T$-value of 3.89 cm^3·K·mol^{-1} (5.58 μ_B) at 295 K, which is close to the spin-only value expected for four uncoupled $S = 1$ ions (4.00 cm^3·K·mol^{-1} 5.66 μ_B, respectively). Figure 9 shows the temperature dependence of the magnetic susceptibility χ_M and the $\chi_M T$ value at a field of 2000 G. By lowering the temperature $\chi_M T$ decreases, indicating an overall antiferromagnetic coupling between the Ni centers. From the molecular structure we can expect two principal magnetic exchange pathways, one intra-dimer coupling via the pyrazolate and the μ-1,1 azide and an inter-dimer coupling between the subunits, which is mediated by the μ-1,3 azide. The experimental data were analyzed by means of the program MAGMUN[20] in a model based on the isotropic exchange Hamiltonian $H = -2J_1(S_2S_3 + S_1S_4) - 2J_2(S_1S_2 + S_3S_4)$ (**A** in Figure 10). The solid line in Figure 9 represents the best fit with $g = 2.01 \pm 0.01$, $J_1 = -16.2 \pm 0.2$ cm^{-1}, $J_2 = +2.0$ cm^{-1}, $\rho = 2.5\%$, $\Theta = 3.5$ K, and $TIP = 2.0 \times 10^{-4}$ cm^3·mol^{-1}.

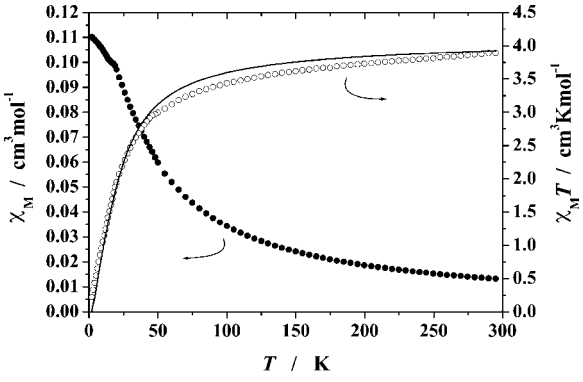

Figure 9. Plot of χ_M (solid circles) and $\chi_M T$ (open circles) vs. T for **3** at 2000 G. The solid line represents the calculated curve fit (see text)

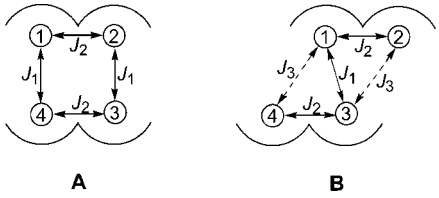

Figure 10. Coupling schemes for **3** (**A**) and **4** (**B**)

In view of the ferromagnetic behavior observed for **1**, it is reasonable to assign J_2 to the coupling within the bimetallic constituents of **3**, and J_1 to the antiferromagnetic inter-dimer exchange mediated by the μ-1,3-N_3 linkages. The intra-dimer coupling is determined by the azide binding mode within the bimetallic pocket and is ferromagnetic as anticipated, its value being of the same order of magnitude as the coupling constant in **1**. Small differences may reflect subtle geometric differences between **1** and the μ-1,1 azido

 © 2004 Wiley-VCH Verlag GmbH & Co. KGaA, Weinheim

bridged building blocks of **3**, in particular the even larger Ni1−N9−Ni2 angle [θ = 118.31(7)°], which is predicted to reduce the ferromagnetic contribution, and the more distinct out-of-plane displacement of the N_3^- ligand in the case of **3**. It should also be noted, that coordination numbers and coordination geometries are quite different for the two dinickel(II) arrays. The inter-dimer antiferromagnetic exchange is in the range expected for a μ-1,3 azide with comparatively wide Ni−N−N angles [141.7(2) and 148.1(2)°] and a torsion of φ = 36.1°.

The $\chi_M T$ value observed for **4** at 295 K is 5.15 $cm^3 \cdot K \cdot mol^{-1}$ (6.42 μ_B). Figure 11 depicts a plot of the temperature dependence of χ_M and $\chi_M T$ at 2000 G. With respect to the topology of **4**, a three-*J* coupling scheme sketched in Figure 10 (**B**) applies. Considering the very long Ni2−N10 bond lengths for the central μ-1,1,3 azido linkages, however, it is reasonable to approximate J_3 as negligible, and that a two-*J* model is adequate for a qualitative analysis of the data. Fitting was carried out with the program MAGMUN[20] based on the isotropic exchange Hamiltonian $H = -2J_1(S_1S_3) - 2J_2(S_1S_2 + S_3S_4)$ (corresponding to **B** and $J_3 = 0$, Figure 10) to give $g = 2.29 \pm 0.02$, $J_1 = -19.7 \pm 0.8$ cm^{-1}, $J_2 = +6.0$ cm^{-1} $\rho = 3.0\%$, $\Theta = 1.8$ K, and $TIP = 3.6 \times 10^{-4}$ $cm^3 \cdot mol^{-1}$ (solid line in Figure 8).

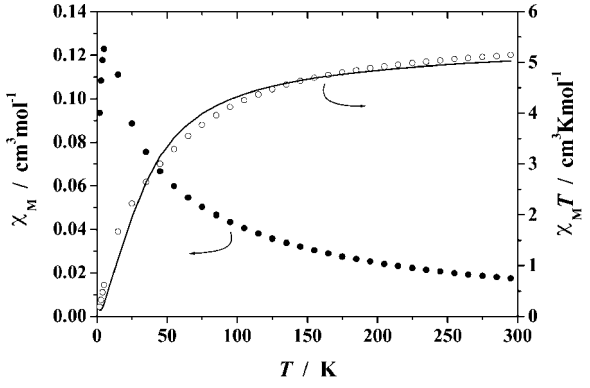

Figure 11. Plot of χ_M (solid circles) and $\chi_M T$ (open circles) vs. *T* for **4** at 2000 G. The solid line represents the calculated curve fit (see text)

Similar to the case of **3**, it would seem appropriate to assign J_2 to the intra-dimer exchange, which is expected to be ferromagnetic, while J_1 should reflect the antiferromagnetic interaction between the two pyrazolate-based subunits. The J_1 value is a little more negative than in the case of **3**, in accordance with the somewhat more acute Ni−N−N angles [Ni1a−N12−N11: 127.4(2)°; Ni1−N10−N11: 133.9(2)°], which are assumed to be the most relevant magnetostructural parameters for a μ-1,3 azido bridge.[6] Likewise, the larger ferromagnetic intra-dimer exchange in **4** may be traced to the much more acute Ni−N−Ni angle for the μ-1,1 azide [Ni1−N7−Ni2: 102.5(1) in **4**].

Conclusion

The present study has established well defined pyrazolate-based dinickel(II) azido complexes as building blocks for the construction of high nuclearity nickel/azido systems. A particular advantage of these compounds is the possibility of tuning the magnetic properties of the bimetallic components, since their spin ground state ($S = 0$ or $S = 2$) is determined by the intra-dimer azide bridging mode, which can be controlled by suitable modifications of the ligand scaffold. Some tetranuclear complexes that arise from the assembly of two Ni_2 subunits are reported in this work as examples. The magnetic exchange within the Ni_2 subunits of the new Ni_4 species is as anticipated and is basically governed by the choice of the building blocks (i.e. ferromagnetic exchange in **1** as well as in **3** and **4**). However, the magnitude of the coupling may differ somewhat, since subtle geometric changes in the subunits occur upon linking the Ni_2 species to give high-nuclearity $\{Ni_2\}_n$ compounds, which represents a general limitation to the prediction of magnetic properties of polynuclear complexes from the magnetic properties of their constituents. Future work will focus on, inter alia, increasing the rigidity of the bimetallic entities and strategies to more efficiently control the linking of the building blocks. In view of the great variety of available dinucleating pyrazolate ligands, we expect a wide range of new oligonuclear and 1D-chain nickel(II) azido systems to be accessible via this precursor based approach.

Experimental Section

Caution! *Although no problems were encountered in this work, transition metal perchlorate and azide complexes are potentially explosive, and should be handled with proper precautions.*

General: Ligands HL^1, HL^2, and HL^3 were prepared as described previously.[10a,21] HPLC grade methanol (CHROMASOLV) was obtained from Riedel-de-Haen. Solvents were dried by established processes. All other chemicals were purchased from commercial sources and used as received. Microanalyses were performed by the Analytisches Labor des Anorganisch-Chemischen Instituts der Universität Göttingen. IR spectra: Digilab Excalibur, recorded as KBr pellets. Mass spectra: Finnigan MAT 95 (FAB-MS). The susceptibility measurements were carried out with a Quantum-Design MPMS-5S SQUID magnetometer equipped with a 5 Tesla magnet in the range of 2 to 300 K. The powdered samples were contained in a gel bucket and fixed in a non-magnetic sample holder. Each raw data file for the measured magnetic moment was corrected for the diamagnetic contribution of the sample holder and the gel bucket. The molar susceptibilities were corrected using the Pascal constant and the increment method according to Haberditzl.[22]

Synthesis of $[L^1Ni_2(\mu\text{-}1,1\text{-}N_3)(NO_3)_2]$ (1): A solution of HL^1 (190 mg, 0.41 mmol) in MeOH (70 mL) was treated with one equivalent of KO*t*Bu (45.7 mg, 0.41 mmol), two equivalents of $Ni(NO_3)2{\cdot}6H_2O$ (236.8 mg, 0.81 mmol), and one equivalent of sodium azide (26.5 mg, 0.41 mmol), and the reaction mixture was stirred at room temperature for 12 h. All volatile materials were then evaporated under reduced pressure and the residue taken up in acetone (60 mL). After filtration, the solution was layered with

 © 2004 Wiley-VCH Verlag GmbH & Co. KGaA, Weinheim

light petroleum to yield green crystals (194 mg, 63%) of the product **1**. MS (FAB+): *m/z* (rel. intensity) = 705 (25) $[L^1Ni_2(NO_3)_2]^+$, 685 (60) $[L^1Ni_2(N_3)(NO_3)]^+$, 665 (25) $[L^1Ni_2(N_3)_2]^+$, 623 (15) $[L^1Ni_2(N_3)]^+$. IR (KBr): $\tilde{\nu}$ = 2939 (w), 2860 (w), 2819 (w), 2767 (w), 2058 (s), 1479 (m), 1385 (vs), 1284 (m), 1234 (w), 1188(w), 1040 (w), 1021(w), 981 (w), 832 (w) cm^{-1}. $C_{25}H_{53}N_{13}Ni_2O_6$ (749.2): calcd. C 40.08, H 7.13, N 24.31; found C 40.28, H 7.23, N 24.78.

Synthesis of $[L^2Ni_2(\mu\text{-}1,3\text{-}N_3)](ClO_4)_2$ (2): A solution of HL^2 (149 mg, 0.285 mmol) in MeOH (70 mL) was treated with one equivalent of KO*t*Bu (32.0 mg, 0.285 mmol), two equivalents of $Ni(ClO_4)2{\cdot}6H_2O$ (208.4 mg, 0.570 mmol), and one equivalent of sodium azide (18.5 mg, 0.285 mmol), and the reaction mixture was stirred at room temperature for 12 h. All volatile materials were then evaporated under reduced pressure and the residue taken up in acetone (50 mL). After filtration the solution was layered with light petroleum to yield green crystals (216 mg, 86%) of the product **2**. MS (FAB+): *m/z* (rel. intensity) = 778 (25) $[L^2Ni_2(N_3)(ClO_4)]^+$, 679 (50) $[L^2Ni_2(N_3)]^+$. IR (KBr): $\tilde{\nu}$ = 2984 (w), 2946 (w), 2884 (w), 2067 (s), 1459 (w), 1388 (w), 1315 (w), 1263 (w), 1092 (vs), 914 (w), 797 (w), 736 (w), 624 (m) cm^{-1}. $C_{29}H_{61}Cl_2N_{11}Ni_2O_8$ (880.2): calcd. C 39.57, H 6.99, N 17.51; found C 39.65, H 7.10, N 17.51.

Synthesis of $[L^1_2Ni_4(\mu\text{-}1,1\text{-}N_3)_2(\mu\text{-}1,3\text{-}N_3)_2](BPh_4)_2{\cdot}2C_3H_6O$ (3·2C_3H_6O): A solution of HL^1 (180 mg, 0.386 mmol) in MeOH (70 mL) was treated with one equivalent of KO*t*Bu (43.3 mg, 0.386 mmol), two equivalents of $Ni(ClO_4)_2{\cdot}6H_2O$ (282.1 mg, 0.771 mmol) and two equivalents of sodium azide (50.2 mg, 0.771 mmol) and was stirred at room temperature for 12 h. All volatile materials were then evaporated under reduced pressure, the residue taken up in ethanol (100 mL), and sodium tetraphenylborate (264 mg, 0.771 mmol) was added. The resultant precipitate was separated by filtration and taken up in acetone (60 mL). The solution was again filtered, and then layered with light petroleum to gradually yield some green crystals (76 mg, 20%) of the product **3**. MS (FAB+): *m/z* (rel. intensity) = 1649 (5) $[L^1_2Ni_4(N_3)_4(BPh_4)]^+$, 665 (100) $[L^1Ni_2(N_3)_2]^+$, 623 (35) $[L^1Ni_2(N_3)]^+$. IR (KBr): $\tilde{\nu}$ = 2964 (m), 2923 (m), 2859 (w), 2129 (s), 2064 (m), 1460 (m), 1384 (s), 1261 (s), 1097 (s), 1032 (s), 803 (s), 732 (w), 703 (w), 612 (w) cm^{-1}. $C_{104}H_{158}B_2N_{28}Ni_4O_2$ (2089.0): calcd. C 59.80, H 7.62, N 18.77; found C 56.42, H 7.18, N 17.68.

Synthesis of $[L^3Ni_2(N_3)_3]_2{\cdot}2CH_2Cl_2$ (4·2CH_2Cl_2): A solution of HL^3 (255 mg, 0.786 mmol) in MeOH (20 mL) was treated with one equivalent of KO*t*Bu (92.7 mg, 0.786 mmol) and two equivalents of $Ni(ClO_4)_2{\cdot}6H_2O$ (580.7 mg, 1.572 mmol). After stirring the mixture for 30 min at room temperature the solution was evaporated to dryness and the residue was taken up in acetone (25 mL). NaN_3 (154.8 mg, 2.358 mmol) was added, and the reaction mixture was stirred for a further 24 h. The green precipitate was separated by filtration then dissolved in dichloromethane (25 mL). Layering the solution with light petroleum (boiling range 40−60 °C, 75 mL) afforded green crystals of the product **4** (148 mg, 29%). MS (FAB+): *m/z* (rel. intensity) = 1088 (16) $[L^3_2Ni_4(N_3)_5]^+$, 523 (100) $[L^3Ni_2(N_3)_2]^+$, 423 (12) $[L^3Ni(N_3)]^+$. IR (KBr): $\tilde{\nu}$ = 3011 (w), 2967 (w), 2909 (w), 2864 (w), 2103 (vs), 2055 (vs), 2037 (vs), 1650 (w), 1472 (m), 1458 (m), 1030 (m), 1009 (w), 826 (w), 669 (w) cm^{-1}. $C_{36}H_{74}Cl_4N_{30}Ni_4$ (1303.8): calcd. C 33.17, H 5.72, N 32.23; found C 33.59, H 5.78, N 32.50.

X-ray Crystallographic Studies: Data collection was carried out with a Bruker AXS CCD diffractometer using graphite-monochromated Mo-K_α radiation (λ = 0.71073 Å). Structures were solved by direct methods (SHELXS-97) and refined by full-matrix least-

Table 2. Crystal data and refinement details for complexes **1**, **2**, **3**, and **4**

	$[L^1Ni_2(\mu\text{-}1,1\text{-}N_3)(NO_3)_2]$ **1**	$[L^2Ni_2(\mu\text{-}1,3\text{-}N_3)](ClO_4)_2$ **2**	$[L^1_2Ni_4(\mu\text{-}1,1\text{-}N_3)_2(\mu\text{-}1,3\text{-}N_3)_2](BPh_4)_2$ **3**	$[L^3Ni_2(N_3)_3]_2$ **4**
Empirical formula	$C_{25}H_{53}N_{13}Ni_2O_6$	$C_{29}H_{61}Cl_2N_{11}Ni_2O_8{\cdot}0.5H_2O$	$C_{98}H_{146}B_2N_{28}Ni_4{\cdot}2C_3H_6O$	$C_{34}H_{70}N_{30}Ni_4{\cdot}2CH_2Cl_2$
Molecular mass (g/mol)	749.22	888.21	2089.04	1303.89
Crystal size (mm)	0.50 × 0.45 × 0.15	0.37 × 0.25 × 0.25	0.40 × 0.23 × 0.20	0.22 × 0.13 × 0.03
Crystal system	monoclinic	monoclinic	triclinic	monoclinic
Space group	$P2_1/n$	$P2_1/n$	$P\bar{1}$	$P2_1/n$
a (Å)	10.3639(5)	11.3834(5)	14.0149(7)	9.8084(5)
b (Å)	33.708(2)	27.6474(2)	14.4822(7)	23.4284(2)
c (Å)	10.6517(6)	12.8429(6)	14.8493(7)	12.3392(7)
α (°)	90	90	97.759(1)	90
β (°)	110.851(1)	99.731(1)	106.411(1)	103.965(1)
γ (°)	90	90	102.041(1)	90
Volume ($Å^3$)	3477.4(3)	3983.8(3)	2766.4(2)	2751.7(3)
$\rho_{calcd.}$ (g/cm^3)	1.431	1.481	1.254	1.574
Z	4	4	1	2
F(000)	1592	1880	1116	1360
Temperature (K)	103(2)	103(2)	297(2)	103(2)
hkl Range	−15 to 14, 0 to 50, 0 to 15	−16 to 16, 0 to 41, 0 to 18	−20 to 18, −20 to 20, 0 to 21	−14 to 14, 0 to 34, 0 to 18
2θ Range (deg)	4.26 to 64.04	4.36 to 64.02	3.14 to 61.02	3.48 to 64.06
Measured reflections	58577	47464	45514	26628
Unique reflections	11942 [*R*(int) = 0.0302]	13577 [*R*(int) = 0.0374]	16829 [*R*(int) = 0.0384]	9476 [*R*(int) = 0.0560]
Obsd. reflections [$I > 2\sigma(I)$]	10821	10666	11612	6267
Refinined params	627	771	925	482
Residual electron density (e $Å^{-3}$)	0.580 and −0.994	1.083 and −0.606	0.516 and −0.339	0.964 and −1.933
*R*1 [$I > 2\sigma(I)$]	0.0397	0.0426	0.0420	0.0531
*wR*2 (all data)	0.0909	0.1074	0.1099	0.1439
Goodness-of-fit	1.222	1.046	1.015	1.065

 © 2004 Wiley-VCH Verlag GmbH & Co. KGaA, Weinheim

squares techniques based on F^2 (SHELXL-97).[23] Atomic coordinates and thermal parameters of the non-hydrogen atoms were refined in fully anisotropic models. Hydrogen atoms were either located in the difference Fourier map or included using the riding model with U_{iso} tied to U_{iso} of the parent atoms. Crystal data and refinement details are listed in Table 2. CCDC-223071 (for **1**), -223072 (for **2**), -223073 (for **3**), and -223074 (for **4**) contain the supplementary crystallographic data for this paper. These data can be obtained free of charge at www.ccdc.cam.ac.uk/conts/retrieving.html or from the Cambridge Crystallographic Data Center, 12 Union Road, Cambridge CB2 1EZ, UK [Fax: (internat.) +44-1223-336-033; E-mail: deposit@ccdc.cam.ac.uk].

Acknowledgments

We sincerely thank the DFG (priority program 1137 "Molecular Magnetism") and the Fonds der Chemischen Industrie for support of this work.

[1] [1a] O. Kahn, *Angew. Chem.* **1985**, *97*, 837−853; *Angew. Chem. Int. Ed. Engl.* **1985**, *24*, 834−850. [1b] O. Kahn, *Molecular Magnetism*, VCH Publishers Inc., New York, **1993**. [1c] J. S. Miller, A. J. Epstein, *Angew. Chem.* **1994**, *106*, 399−432; *Angew. Chem. Int. Ed. Engl.* **1994**, *33*, 385−415. [1d] *Molecule-Based Magnetic Materials* (Eds.: M. M. Turnbull, T. Sugimoto, L. K. Thompson), ACS Symposium Series 644, Washington, **1996**.

[2] *Magnetism: Molecules to Materials* (Eds.: J. S. Miller, M. Drillon), Wiley-VCH, Weinheim, **2001**.

[3] [3a] R. Sessoli, H.-L. Tsai, A. N. Schake, S. Wang, J. B. Vincent, K. Folting, D. Gatteschi, G. Christou, D. N. Hendrickson, *J. Am. Chem. Soc.* **1993**, *115*, 1804−1816. [3b] A. K. Powell, S. L. Heath, D. Gatteschi, L. Pardi, R. Sessoli, G. Spina, F. Del Giallo, F. Pieralli, *J. Am. Chem. Soc.* **1995**, *117*, 2491−2502. [3c] A. Müller, F. Peters, M. T. Pope, D. Gatteschi, *Chem. Rev.* **1998**, *98*, 239−271. [3d] D. Gatteschi, R. Sessoli, A. Cornia, *Chem. Commun.* **2000**, 725−732. [3e] J. Larionova, M. Gross, M. Pilkington, H. Andres, H. Stoeckli-Evans, H. U. Güdel, S. Decurtins, *Angew. Chem.* **2000**, *112*, 1667−1672; *Angew. Chem. Int. Ed.* **2000**, *39*, 1605−1609.

[4] [4a] O. Kahn, *Metal-Organic and Organic Molecular Magnets*, Spec. Publ. 252, Royal Society of Chemistry, **2000**, 150−168. [4b] O. Kahn, J. Larionova, L. Ouahab, *Chem. Commun.* **1999**, 945−952. [4c] A. Caneschi, D. Gatteschi, C. Sangregorio, R. Sessoli, L. Sorace, A. Cornia, M. A. Novak, C. Paulsen, W. Wernsdorfer, *J. Magn. Magn. Mater.* **1999**, *200*, 182−201.

[5] [5a] M.-F. Charlot, O. Kahn, M. Chaillet, C. Larrieu, *J. Am. Chem. Soc.* **1986**, *108*, 2574−2581. [5b] L. K. Thompson, S. S. Tandon, *Comments, Inorg. Chem.* **1996**, *18*, 125−144.

[6] J. Ribas, A. Escuer, M. Monfort, R. Vicente, R. Cortés, L. Lezama, T. Rojo, *Coord. Chem. Rev.* **1999**, *193−195*, 1027−1068.

[7] [7a] M. A. Halcrow, J. C. Huffman, G. Christou, *Angew. Chem.* **1995**, *107*, 971−973; *Angew. Chem. Int. Ed. Engl.* **1995**, *34*, 889−891. [7b] M. A. Halcrow, J.-S. Sun, J. C. Huffman, G. Christou, *Inorg. Chem.* **1995**, *34*, 4167−4177. [7c] M. W. Wemple, D. M. Adams, K. S. Hagen, K. Folting, D. N. Hendrickson, G. Christou, *J. Chem. Soc., Chem. Commun.* **1995**, 1591−1593. [7d] D. Ma, S. Hikichi, M. Akita, Y. Moro-oka, *J. Chem. Soc., Dalton Trans.* **2000**, 1123−1134. [7e] M. A. S. Goher, J. Cano, Y. Journaux, M. A. M. Abu-Youssef, F. A. Mautner, A. Escuer, R. Vicente, *Chem. Eur. J.* **2000**, *6*, 778−784.

[8] G. S. Papaefstathiou, S. P. Perlepes, A. Escuer, R. Vicente, M. Font-Bardia, X. Solans, *Angew. Chem.* **2001**, *113*, 908−910; *Angew. Chem. Int. Ed.* **2001**, *40*, 884−886.

[9] F. Meyer, P. Kircher, H. Pritzkow, *Chem. Commun.* **2003**, 774−775.

[10] [10a] F. Meyer, S. Beyreuther, K. Heinze, L. Zsolnai, *Chem. Ber./Recueil* **1997**, *130*, 605−613. [10b] F. Meyer, K. Heinze, B. Nuber, L. Zsolnai, *J. Chem. Soc., Dalton Trans.* **1998**, 207−213. [10c] F. Meyer, P. Rutsch, *Chem. Commun.* **1998**, 1037−1038. [10d] F. Meyer, E. Kaifer, P. Kircher, K. Heinze, H. Pritzkow, *Chem. Eur. J.* **1999**, *5*, 1617−1630. [10e] J. Ackermann, F. Meyer, E. Kaifer, H. Pritzkow, *Chem. Eur. J.* **2002**, *8*, 247−258.

[11] F. Meyer, U. Ruschewitz, P. Schober, B. Antelmann, L. Zsolnai, *J. Chem. Soc., Dalton Trans.* **1998**, 1181−1186.

[12] F. Meyer, H. Pritzkow, *Inorg. Chem. Commun.* **2001**, *4*, 305−307.

[13] The angular structural parameter τ is defined as $\tau = (\beta - \alpha)/60$, where α and β represent two basal angles with $\beta > \alpha$. It is a measure of the degree of trigonality: A perfect TB-5 structure is associated with $\tau = 1$, while $\tau = 0$ is expected for an idealized SPY-5 geometry; A. W. Addison, T. N. Rao, J. Reedijk, J. van Rijn, G. C. Verschoor, *J. Chem. Soc., Dalton Trans.* **1984**, 1349−1356.

[14] F. Meyer, R. F. Winter, E. Kaifer, *Inorg. Chem.* **2001**, *40*, 4597−4603.

[15] B. Kersting, G. Steinfeld, D. Siebert, *Chem. Eur. J.* **2001**, *7*, 4253−4258.

[16] [16a] M. Montfort, J. Ribas, X. Solans, *J. Chem. Soc., Chem. Commun.* **1993**, 350. [16b] J. Ribas, M. Montfort, X. Solans, M. Drillon, *Inorg. Chem.* **1994**, *33*, 742. [16c] I. Agrell, *Acta Chem. Scand.* **1967**, *21*, 2647. [16d] M. A. S. Goher, A. Escuer, M. A. M. Abu-Youssef, F. A. Mautner, *Polyhedron* **1998**, *17*, 4265.

[17] [17a] C. G. Pierpont, D. N. Hendrickson, D. M. Duggan, F. Wagner, E. K. Barefield, *Inorg. Chem.* **1975**, *14*, 604−610. [17b] F. Wagner, M. T. Mocella, M. J. J. D′Aniello, A. H. J. Wang, E. K. Barefield, *J. Am. Chem. Soc.* **1974**, *96*, 2625−2627. [17c] G. A. McLachlan, G. D. Fallon, R. L. Martin, B. Moubaraki, K. S. Murray, L. Spiccia, *Inorg. Chem.* **1994**, *33*, 4663−4668. [17d] L. Fabbrizzi, P. Pallavicini, L. Parodi, A. Perotti, N. Sardone, A. Taglietti, *Inorg. Chim. Acta* **1996**, *244*, 7−9. [17e] A. Escuer, C. J. Harding, Y. Dussart, J. Nelson, V. McKee, R. Vicente, *J. Chem. Soc., Dalton Trans.* **1999**, 223−228. [17f] Z.-H. Zhang, X.-H. Bu, Z.-H. Ma, W.-M. Bu, Y. Tang, Q.-H. Zaho, *Polyhedron* **2000**, *19*, 1559−1566.

[18] F. Meyer, H. Kozlowski, in *Comprehensive Coordination Chemistry II* (Eds.: J. A. McCleverty, T. J. Meyer), Pergamon, **2004**, vol. 6, 247−554.

[19] E. Ruiz, J. Cano, S. Alvarez, P. Alemany, *J. Am. Chem. Soc.* **1998**, *120*, 11122−11129.

[20] The fits for the tetranuclear complexes **3** and **4** were performed by the program MAGMUN. This program has been developed by Dr. Z. Xu in collaboration with Prof. L. K. Thompson and Dr. O. Waldmann. The program is available free of charge from the authors. See also: L. K. Thompson, O. Waldmann, Z. Xu, in *Magnetism: Molecules to Materials IV* (Eds.: J. S. Miller, M. Drillon), Wiley-VCH, Weinheim, **2002**, p. 173−202.

[21] J. C. Röder, F. Meyer, M. Konrad, S. Sandhöfner, E. Kaifer, H Pritzkow, *Eur. J. Org. Chem.* **2001**, 4479−4487.

[22] [22a] W. Haberditzel, *Angew. Chem.* **1966**, *78*, 277−288; *Angew. Chem. Int. Ed. Engl.* **1966**, *5*, 288−299. [22b] W. Haberditzel, *Magnetochemie*, Akademie-Verlag, Berlin, **1968**.

[23] G. M. Sheldrick, SHELXS-97, *Program for Crystal Structure Solution*, University of Göttingen, **1997**; G. M. Sheldrick, SHELXL-97, *Program for Crystal Structure Refinement*, University of Göttingen, **1997**.

Received November 10, 2003
Early View Article
Published Online April 26, 2004

 © 2004 Wiley-VCH Verlag GmbH & Co. KGaA, Weinheim